Electronic Supplementary Information

Modulating Electrolyte Solvation Structure with Fe-Embedded Carbon Matrix Substrates for Robust Lithium-Metal Plating

Jiayue Peng, *[a, b] Jinghan Wang, [b] Xiangjun Pu, [b] and Jia Xie*[a]

[a] State Key Laboratory of Advanced Electromagnetic Technology, School of Electrical and Electronic Engineering, Huazhong University of Science and Technology, Wuhan 430074, Hubei, China

[b] Department of Materials Science and Engineering, Seoul National University, Seoul, Republic of Korea

* E-mails: xiejia@hust.edu.cn., jiayue_peng@hust.edu.cn

1. Experimental Section

1.1. Materials

Iron-1,3,5-benzenetricarboxylate (Fe-BTC, Basolite F-300), fluoroethylene carbonate (FEC, 99%), diethyl carbonate (DEC, >99%) and lithium bis(fluorosulfonyl)imide (LiFSI, 99.9%) were purchased from Sigma-Aldrich without further purification. FEC and DEC were dehydrated by 4 Å molecular sieves for at least 48h. LiFSI was dried at 90°C under vacuum oven over 24h.

1.2. Synthesis of Fe@C powder

Iron nanoparticles encapsulated in a porous carbon framework (denoted as Fe@C) were synthesized through the pyrolysis of Fe-BTC. Initially, Fe-BTC underwent an activation process at 150°C for 24 hours within a vacuum oven. Subsequently, this activated Fe-BTC powder was subject to an annealing procedure at 500°C for 4 hours under N_2 atmosphere, and the ramp rate was 2°C /min. Prior to exposure to the ambient environment, each sample was passivated at room temperature using a 5% O_2/N_2 mixture for 2 hours. Through this methodology, Fe-BTC underwent carbonization and reduction, resulting in the formation of the Fe@C composite.

1.3. Materials characterization

Powder X-ray diffraction spectra were obtained using a D2 PHASER (Bruker) equipped with CuKα radiation (λ = 1.54178 Å). SEM images were captured using a Zeiss Merlin High-resolution Scanning Electron Microscope operating at 3 kV. The SEM samples were ionic sputtered with a Pt layer to minimize charging effects. FTIR spectra were recorded on a PerkinElmer Spectrum Two FTIR spectrophotometer. XPS

data were gathered using a Thermo Scientific Nexsa G2 X-Ray Photoelectron Spectrometer without any exposure to moisture and air. The XPS spectra were calibrated based on the C 1s peak at 284.5 eV, which corresponds to C-C bonding. The Brunauer–Emmett–Teller surface area was measured using a Micromeritics 3Flex analyser (77 K and 1 atm). All tested electrodes were washed three times with DMC solvent and further dried in the glovebox chamber for 20 min.

1.4. Electrochemical measurements

1.4.1 Electrode preparation

For the anode, a homogeneous slurry was prepared by mixing Fe@C (80 wt%), Super P (10 wt%), and polyacrylonitrile (PAN, 10 wt%) in NMP solvent. This slurry was uniformly spread onto copper foil and subsequently dried in a 120°C oven. The prepared Fe@C electrode and bare Cu foil were cut into 12.7 mm diameter discs and dried in a vacuum at 70°C overnight.

For the cathode, a slurry comprising $LiNi_{0.5}Co_{0.2}Mn_{0.3}$ (NCM523), Super P, and PVDF in a 90:5:5 weight ratio was dispersed in NMP solvent. This mixture was then coated onto an aluminum foil and dried under vacuum at 70°C overnight. The mass loading of NCM523 in each electrode was approximately 10 mg cm^{-2}.

1.4.2 Battery fabrication and testing

The electrolyte used was 1.2 M LiFSI in a FEC/DEC solution mixed in a 1:2 volume ratio. The 2032-coin cells were assembled in an argon-filled glovebox (with O_2 and H_2O content below 0.1 ppm), using PP separators (Celgard 2400) with a 16.5 mm diameter.

Coulombic efficiency (CE) for Li plating/stripping was determined using Li-Cu and Li-Fe@C cells. Here, Li was plated at a fixed capacity of 1.0 mAh cm^{-2} and stripped at a cut-off voltage of 1.0 V with a current density of 1.0 mA cm^{-2}. The performance of Cu-NCM523 and Fe@C-NCM523 cells was evaluated between 3.0 and 4.3 V at 0.1 C and 0.5 C rates, respectively (the first two cycles for the Fe@C-NCM523 cell were conducted at 0.1 C). The Li@Cu-NCM523 and Li@Fe@C-NCM523 cell, assembled using a lithiated Cu and lithiated Fe@C electrode with a fixed capacity of 1 mAh cm^{-2}, underwent initial cycling at 0.1C between 3.0 and 4.3 V, followed by subsequent cycles at 0.5C. These cells were cycled galvanostatically on a WonTech battery test system at 25°C. Electrochemical impedance spectroscopy (EIS) measurements were conducted using a Bio-logic VSP over a frequency range of 10 mHz to 1 MHz, with an AC signal amplitude of 5 mV.

1.5 Computational details

All quantum chemistry calculations were conducted using the Gaussian 09 package[1] to conduct analyses of the lowest unoccupied molecular orbital (LUMO), highest occupied molecular orbital (HOMO) and natural bond orbitals (NBO). The geometries of molecules and Li-solvent-anion complexes were first optimized using the B3LYP-D3(BJ) functional in combination with 6-311++G(d,p) basis set[2]. All the optimized structures were confirmed as potential minima, with no frequency modes with imaginary eigenvalues, through frequency analyses following geometry optimizations. The energies were obtained through M06-2X(D3) functional with DEF2TZVP basis set[3, 4]. In order to make the computational results closer to the actual electrolyte, the

solvent tetrahydrofuran was adopted. The solvation effect was considered using the universal solvation model of SMD[5].

DFT calculations for Fe-BTC and Fe-BTC complexes were performed using the Vienna Ab initio Simulation Package (VASP)[6, 7]. The exchange-correlation interactions were described using the Perdew-Burke-Ernzerhof (PBE) functional within the generalized gradient approximation (GGA)[8]. Core-electron interactions were modeled using the projector augmented wave (PAW) method[9, 10], and a plane-wave basis set was employed with a kinetic energy cutoff of 400 eV. The Brillouin zone was sampled using a Gamma-centered k-point grid with a 3×3×3 mesh, ensuring appropriate convergence.
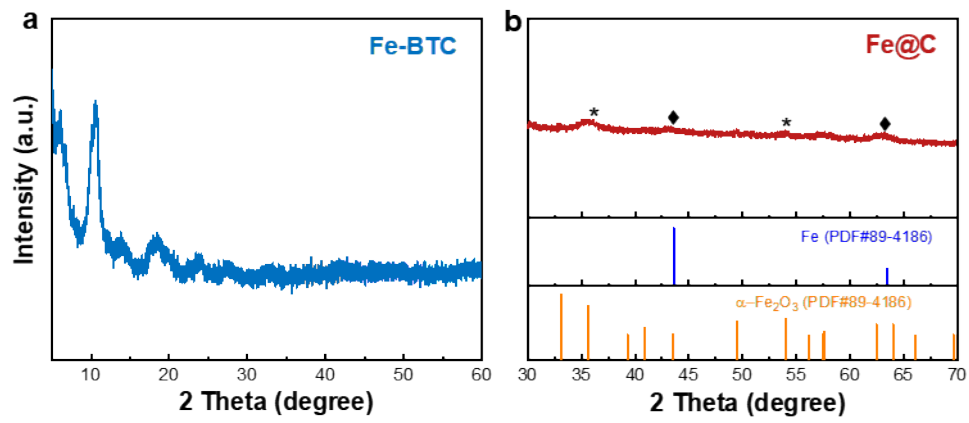
Figure S1. XRD patterns of pristine Fe-BTC (a) and carbonized Fe@C (b).
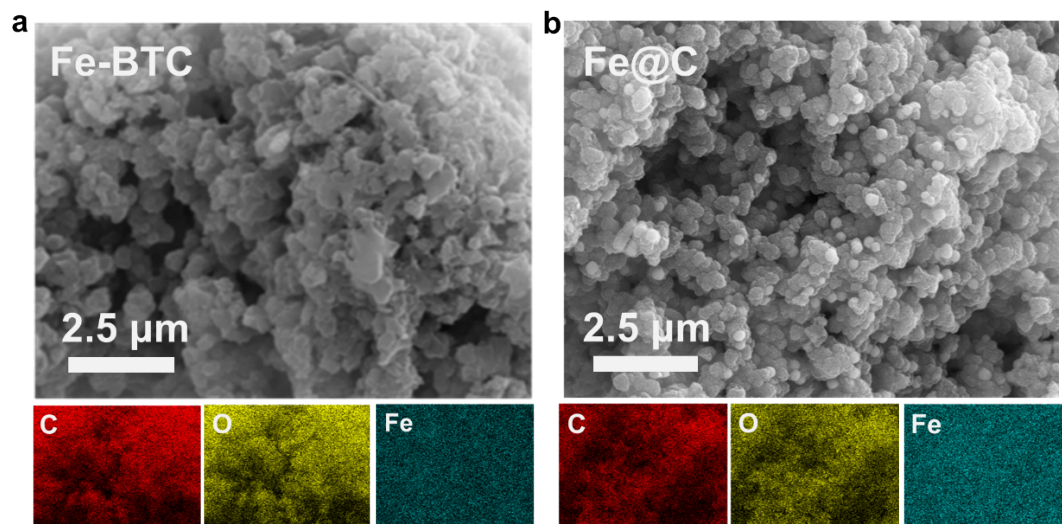
Figure S2. SEM images and EDX mappings of distribution C, O, Fe elements for Fe-BTC (a) and Fe@C (b).
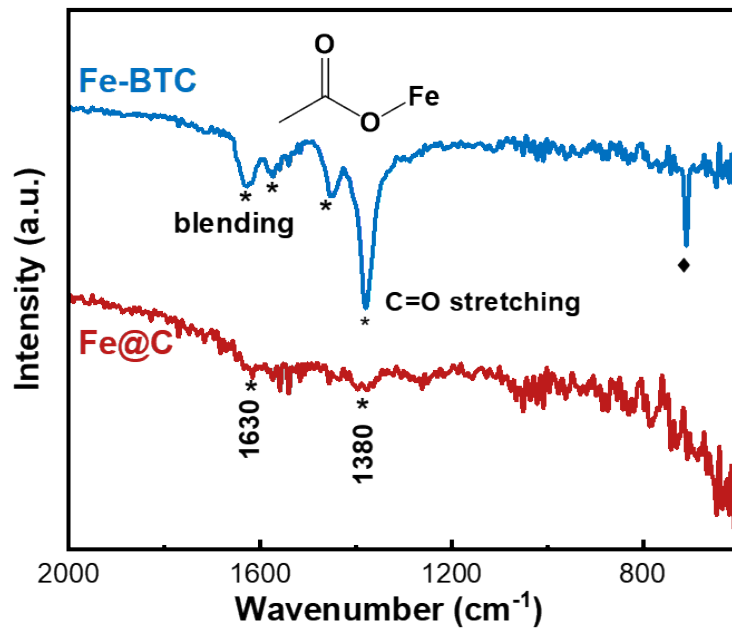
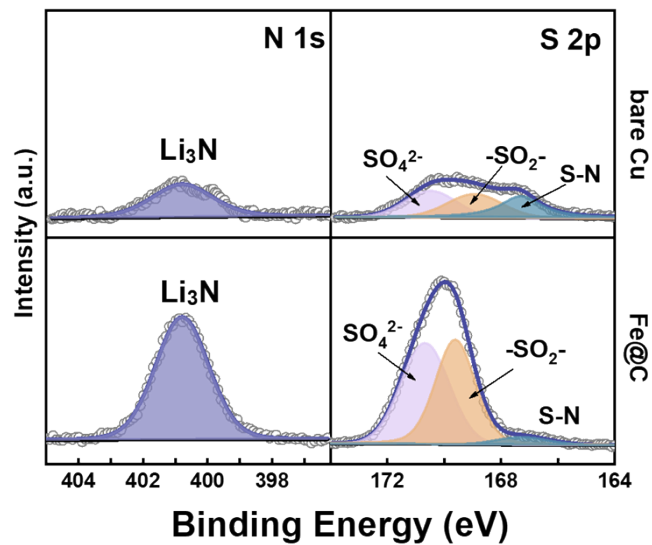**Figure S3.** FTIR spectra of Fe-BTC and Fe@C.

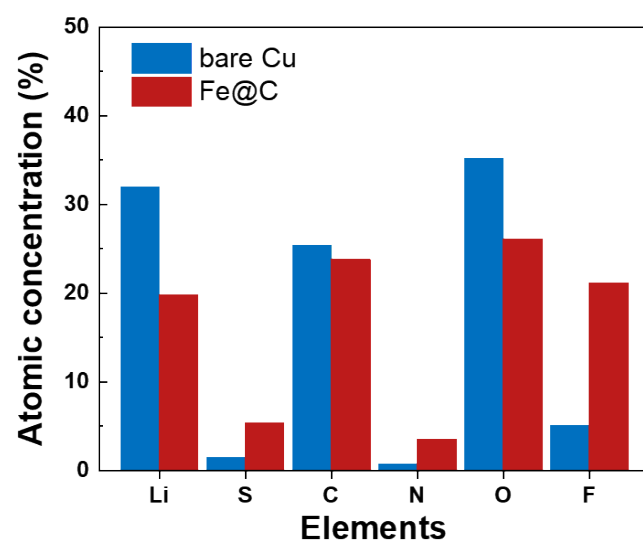**Figure S4.** XPS N1s and S 2p spectra of Li metal deposited on bare Cu foil and Fe@C electrode.

Figure S5. The atomic ratios of Li, C, N, O, F and S in the XPS analysis of deposited Li.
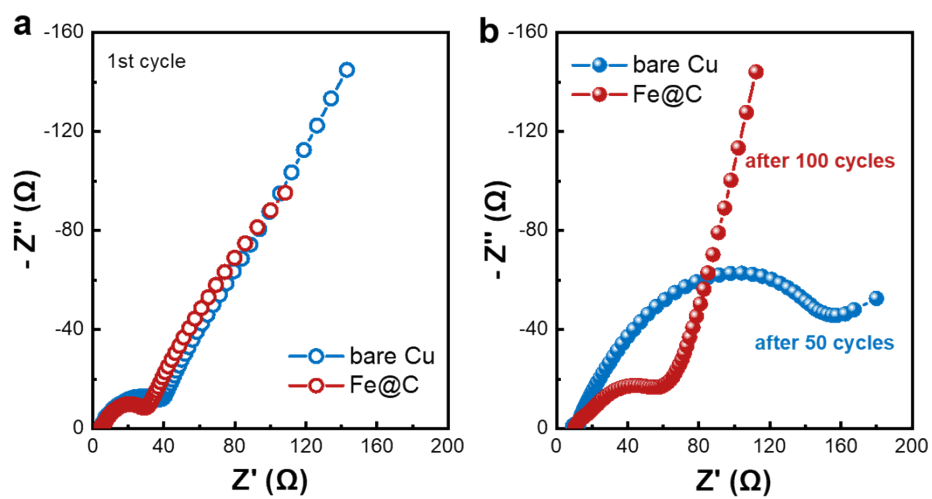
Figure S6. Nyquist plots of half cells after (a) 1 cycle and (b) 50 cycles (bare Cu foil) and 100 cycles (Fe@C electrode).

a

$E_{min} = -45.38$ kcal/mol
$E_{max} = 213.20$ kcal/mol

b

$E_{min} = -34.40$ kcal/mol
$E_{max} = 222.02$ kcal/mol

c

$E_{min} = -38.45$ kcal/mol
$E_{max} = 17.82$ kcal/mol

d

$E_{min} = -41.33$ kcal/mol
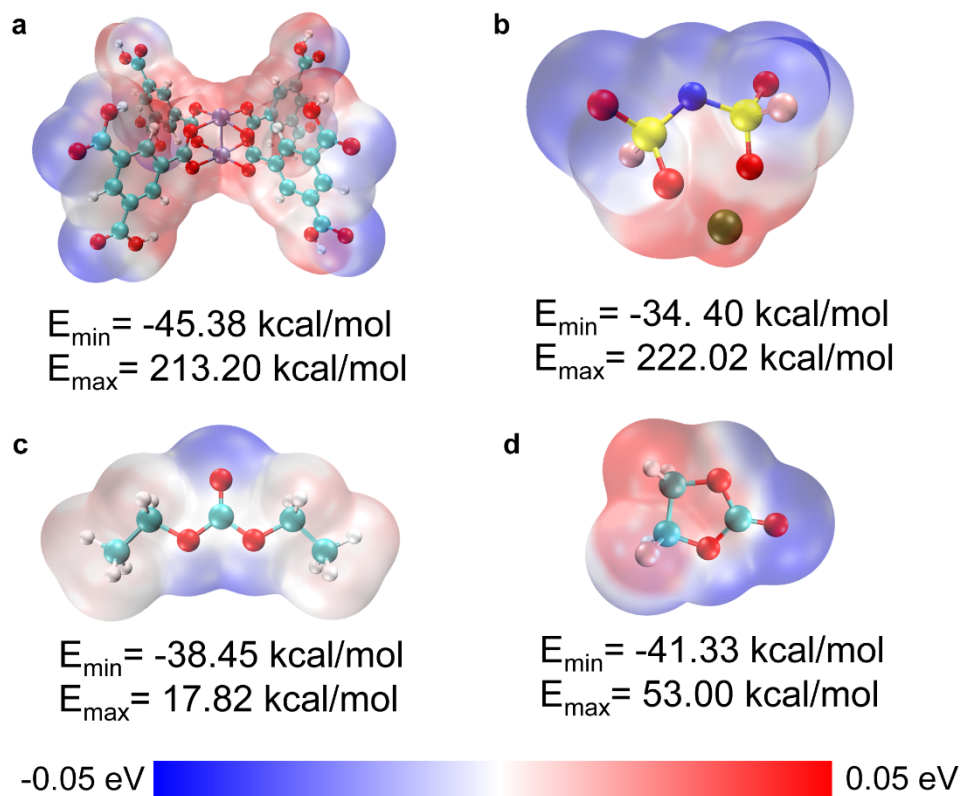$E_{max} = 53.00$ kcal/mol

-0.05 eV ⟶ 0.05 eV

Figure S7. Electrostatic potential (ESP) mapped molecular van der Waals (vdW) surface of the (a) Fe-BTC, (b) Li-FSI, (c) DEC and (d) FEC.
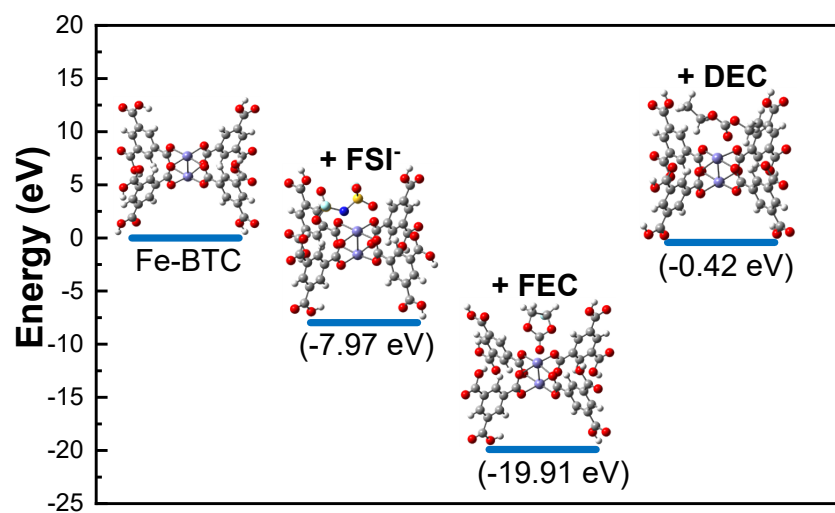
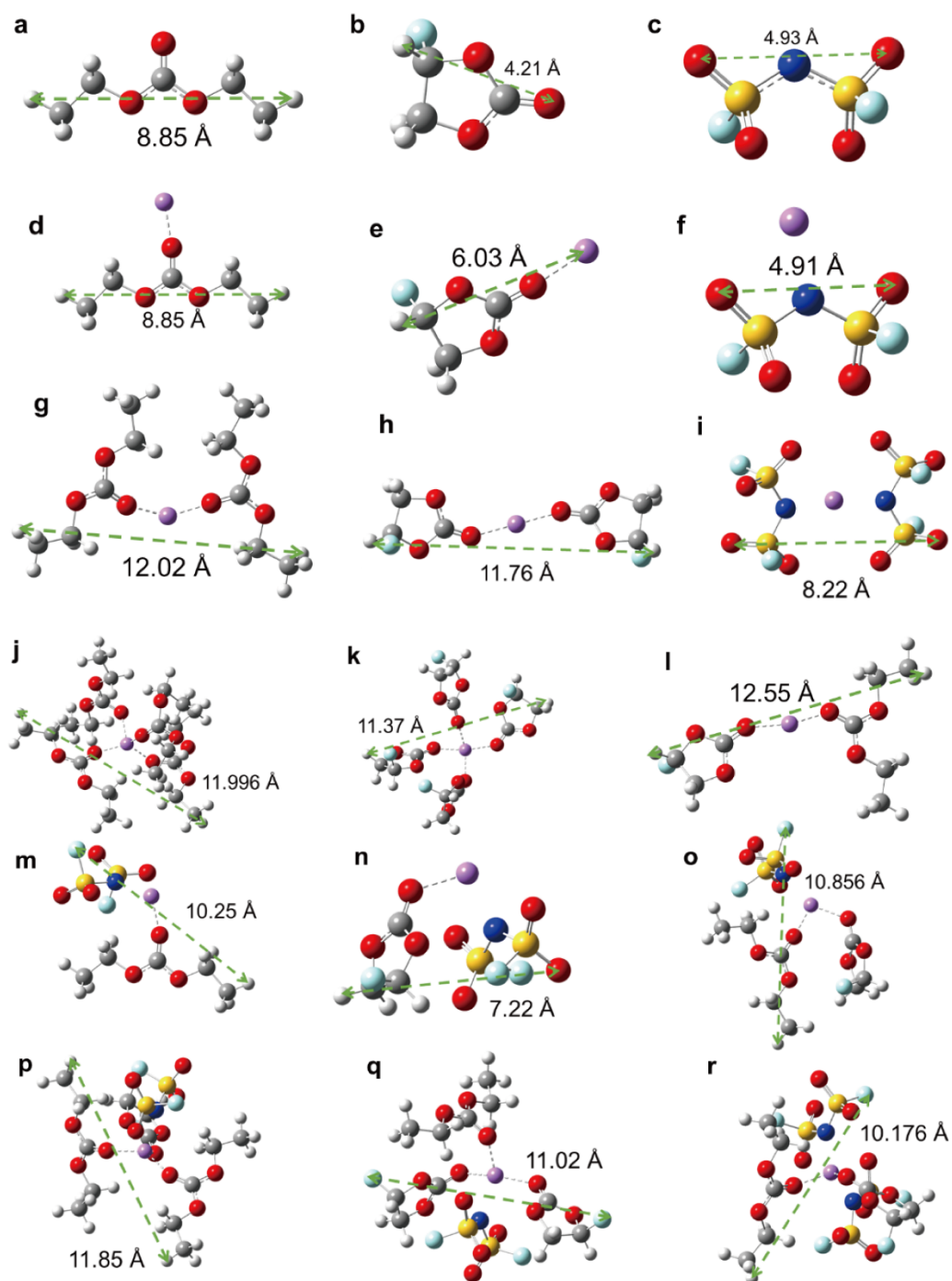**Figure S8.** Energy comparisons of Fe-BTC with FSI⁻, FEC and DEC.

Figure S9. The optimized structure of (a) DEC, (b) FEC, (c) FSI⁻, (d) Li⁺-DEC, (e) Li⁺-FEC, (f) Li⁺-FSI-, (g) Li⁺-2DEC, (h) Li⁺-2FEC, (i) Li⁺-2FSI-, (j) Li⁺-4DEC, (k) Li⁺-4FEC, (l) Li⁺-FEC/DEC, (m) Li⁺-DEC-FSI-, (n) Li⁺-FEC-FSI-, (o) Li⁺-FEC/DEC-FSI-, (p) Li⁺-FEC/2DEC-FSI⁻, (q) Li⁺-2FEC/DEC-FSI⁻ and (r) Li⁺-FEC/DEC-2FSI⁻. White, pink, grey, blue, red, cyan and yellow balls represent H, Li, C, N, O, F and S atoms, respectively.
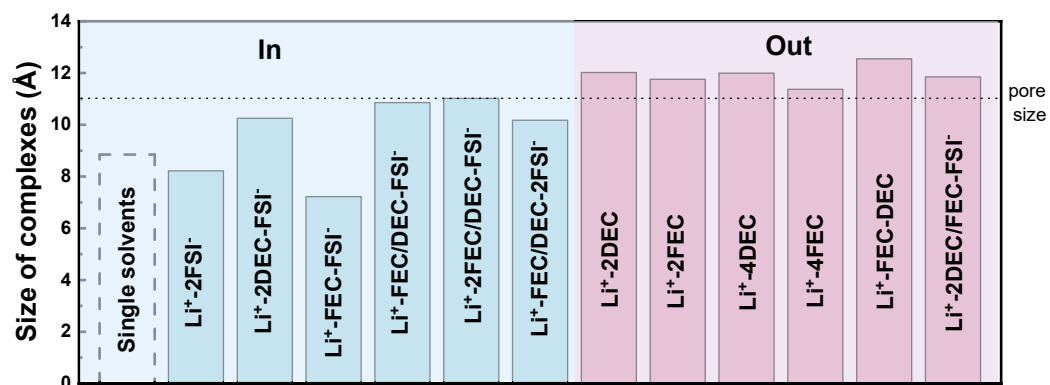
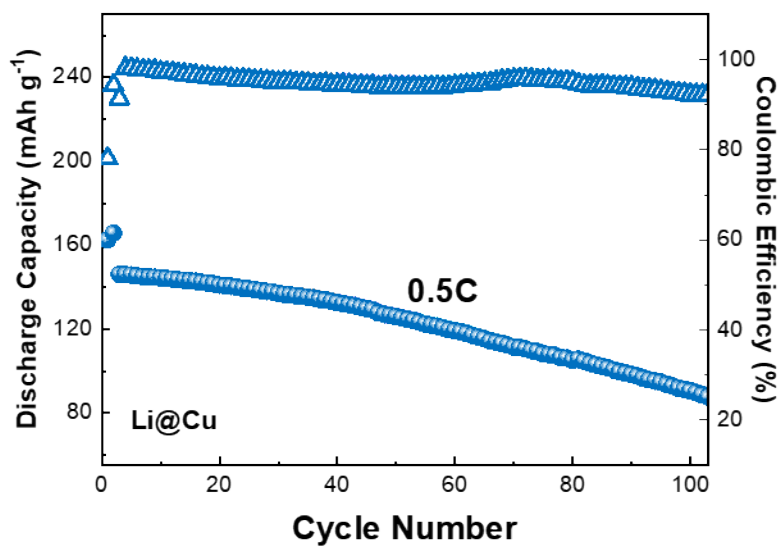**Figure S10.** Analysis of calculated sizes for different solvation complexes.

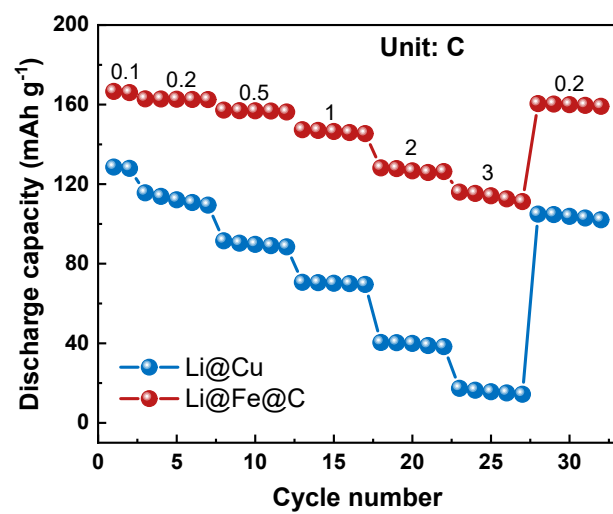**Figure S11.** The discharge and CE of Li@Cu-NCM523 full cell.

Figure S12. Rate performance of Li-NCM523 full cells with different electrodes.

Table S1. Surface composition of Fe-BTC and Fe@C obtained from EDX

Sample	C (wt%)	O (wt%)	Fe (wt%)
Fe-BTC	50.47	34.12	15.41
Fe@C	47.54	25.85	26.61

Table S2. Variations of Brunauer–Emmett–Teller (BET) surface area, Barrett–Joyner–Halenda (BJH) total mesopore volume and t-plot total micropore volume

Sample	BET Specific Surface Area (m^2/g)	BJH Mesopore Volume (cm^3/g)	t-Plot Micropore Volume (cm^3/g)
Fe-BTC	1443.83	0.277	0.588
Fe@C	596.6	0.015	0.232

References

1. M. Frisch, G. Trucks, H. Schlegel, G. Scuseria, M. Robb, J. Cheeseman, G. Scalmani, V. Barone, B. Mennucci and G. Petersson, 2013.
2. A. D. J. T. J. o. c. p. Becke, 1992, **96**, 2155-2160.
3. R. Banerjee, A. Phan, B. Wang, C. Knobler, H. Furukawa, M. O'Keeffe and O. M. Yaghi, 2008, **319**, 939-943.
4. F. Weigend and R. J. P. C. C. P. Ahlrichs, 2005, **7**, 3297-3305.
5. A. V. Marenich, C. J. Cramer and D. G. J. T. J. o. P. C. B. Truhlar, 2009, **113**, 6378-6396.
6. G. Kresse and J. J. P. r. B. Hafner, 1993, **47**, 558.
7. G. Kresse and J. J. P. r. B. Furthmüller, 1996, **54**, 11169.
8. J. P. Perdew, A. Ruzsinszky, G. I. Csonka, O. A. Vydrov, G. E. Scuseria, L. A. Constantin, X. Zhou and K. J. P. r. l. Burke, 2008, **100**, 136406.
9. J. P. Perdew and Y. J. P. r. B. Wang, 1992, **45**, 13244.
10. G. Kresse and D. J. P. r. b. Joubert, 1999, **59**, 1758.